Biointerface Research in Applied Chemistry
Open-Access Journal (ISSN: 2069-5837)

Article
Volume 15, Issue 4, 2025, 50
https://doi.org/10.33263/BRIAC154.050

Flavonoids as Modulators of Sirtuin-6 for Management of Metabolic Syndrome: An *In Silico* Approach

Arjun Singh Kaushik [1], Vipul Agarwal [2], Mujeeba Rehman [1], Rishabh Chaudhary [1], Siddhi Srivastava [1], Sukriti Srivastava [1], Ajay Mahor [3], Vikas Mishra [1,*]

[1] Department of Pharmaceutical Sciences, Babasaheb Bhimrao Ambedkar University, Vidya Vihar Raebareli Road, Lucknow 226025, Uttar Pradesh, India
[2] MIT College of Pharmacy, Ram Ganga Vihar Phase-II, Moradabad, 244001, (U.P.), India
[3] Amity Institute of Pharmacy, Amity University, Gwalior- 474005, Madhya Pradesh, India
* Correspondence: vikasmishra12@gmail.com; dr.vikasmishra@bbau.ac.in

Received: 9.12.2024; Accepted: 19.05.2025; Published: 21.07.2025

Abstract: Sirtuin 6 (SIRT6), a member of the sirtuin family, regulates various cellular processes involved in aging, metabolism, and cancer. Dysregulation of SIRT6 has been widely observed in metabolic syndrome (MS), and some chemical activators of SIRT6 have shown therapeutic success. There is a need to explore natural compounds with SIRT6 activator activity that are affordable and have fewer side effects. The aim of this study was to identify novel compounds targeting SIRT6 and provide a new approach for developing therapies for MS. A library of 239 flavonoid compounds was docked against SIRT6 (PDB ID-3ZG6) using the Schrödinger Glide Module. Based on docking scores, the top 12 flavonoid compounds with promising binding affinities (docking score <-10.26) were identified and subjected to ADMET profiling using SwissADME and pkCSM. ADMET profiling demonstrated that two flavonoid compounds, Isosilybin and Tilianin, possess excellent drug-like properties, suggesting their potential as allosteric SIRT6 activators. The interactions between these compounds were further validated by MM-GBSA and molecular dynamics (MD) using Prime and Desmond of the Schrödinger Suite. MM-GBSA and MD revealed that both the selected flavonoid compounds exhibited strong protein-ligand interactions, indicating their potential as SIRT6 activators. This study provides evidence for the effectiveness of these flavonoid compounds as potent SIRT6 activators.

Keywords: flavonoids; molecular docking; ADMET screening; SIRT6; MM-GBSA; molecular dynamics.

1. Introduction

Sirtuins are NAD-dependent, evolutionarily conserved class III deacetylase enzymes. Their roles in various human diseases have been intensively studied [1]. There are seven members of the sirtuin family in mammals (SIRT1-7), each of which performs a unique function and is localized in a different part of the cell [2]. Their central catalytic core consists of 275 amino acids and is separated from the N- and C-terminal regions, both of which can vary in length and sequence [3]. The crystal structures of the sirtuin catalytic core regions are known, consisting of two domains: a larger, structurally homologous Rossmann-fold domain and a smaller, more diverse Rossmann-fold domain that binds zinc [4]. The cofactor NAD+ and acetyl-lysine-containing peptide substrate enter from the opposite sides of the cleft formed

by the loops connecting these domains and bind to the enzyme. Additionally, in the sirtuin family, the amino acids in the cleft between the two domains have the highest sequence conservation [5].

SIRT6 exhibits mono-ADP ribosyltransferase and deacylase activities in addition to deacetylating histone 3 lysine 9 (H3K9) and 56 (H3K56). SIRT6-H3K9-myristoylated peptide crystallization indicates that substrate occupancy in the hydrophobic pocket can cause the N-terminal region (1-12 residues) to become organized [6,7]. This is in contrast to the SIRT6-ADPr complex structure, in which a high density of residues is not observed [8]. Additionally, SIRT6 is superior to acetylated peptides in hydrolyzing long-chain fatty acyl-lysine [9]. SIRT6 is abundant in the synaptosomal membrane fraction and is substantially expressed in cortical and hippocampal areas of the brain [10]. SIRT6 knockout mice exhibit metabolic abnormalities, rapid aging, and die early [11]. Brain-specific Mice lacking SIRT6 can survive, but the absence of SIRT6 causes neurodegeneration by increasing DNA damage, apoptosis, and toxic Tau phosphorylation [11,12]. SIRT6 has also been shown to preferentially interact with telomeres, and its deficiency leads to telomere malfunction, including end-to-end chromosomal fusion and early cellular senescence. Furthermore, SIRT6-depleted cells exhibit an aberrant telomere structure, similar to the abnormalities observed in Werner syndrome, a premature aging disorder [7,13].

The majority of sirtuin modulators discovered thus far have been identified through screening of natural chemical libraries [14]. The crystal structures of the catalytic domain of SIRT6 (12-296), which contains the non-hydrolyzable cofactor analog ADP-ribose (ADPr) in association with modulators, have been described over the past five years [15]. Although several small-molecule SIRT6 activators have been reported in recent years, such as MDL-800, UBCS039, MDL-811, Quercetin, and Resveratrol, only a few have advanced to animal studies. These synthetic and natural compounds have shown promising effects in modulating epigenetic regulation, oxidative stress, and glucose metabolism [16–19]. For instance, MDL-800 binds allosterically to SIRT6, enhancing its deacetylase activity on H3K9 and H3K56, and has demonstrated significant efficacy in preclinical cancer models. Despite these advances, there remains a notable gap in the identification of natural product-based SIRT6 activators [17,20]. The present study aims to bridge this gap by exploring flavonoids as natural, potentially safer SIRT6 modulators with therapeutic relevance.

2. Materials and Methods

2.1. Docking studies.

The docking study was carried out on a Lenovo desktop machine equipped with Ubuntu OS, Intel® Xeon® processor, and Intel graphics using Maestro 11.0.015 (Small-Molecule Drug Discovery Suite 2018-4, Schrödinger, LLC, New York, NY, 2018) [21].

2.1.1. Protein preparation.

The crystal structure of SIRT6 (PDBID: 3ZG6) was downloaded from the Protein Data Bank (https://www.rcsb.org/structure/3zg6) at a resolution of 2.20 Å, and was pre-processed using Protein Preparation Wizard in Schrödinger suite (Schrödinger Release 2018-4: Protein Preparation Wizard; Epik, Schrödinger, LLC, New York, NY, 2018). The bonding orders were determined using the CCD database, and the appropriate hydrogen atoms were added. The Prime module (Schrödinger Release 2018-4: Prime, Schrödinger, LLC, New York, NY, 2018)

was used to insert missing side chains and loops. Epik was used to produce the hetero state at pH 7.0, and disulfide linkages were constructed with zero bond order. The atoms were removed from the protein structure. In addition, we optimized hydrogen bonds using the refine tab to correct flaws in the protein structure, and then minimized the protein using the OPLS 2005 force field after deleting water molecules with fewer than three hydrogen bonds to non-water molecules [21].

2.1.2. Ligand preparation.

A library of 239 flavonoid compounds was downloaded from MedChemExpress (https://www.medchemexpress.com) and processed using the LigPrep module in the Schrödinger suite (Schrödinger Release 2018-4: LigPrep, Schrödinger, LLC, New York, 2018). The Epik module was used to produce optimal states at pH 7±2 and to manufacture the tautomers. Each ligand preserved up to 32 stereoisomers [22,23].

2.1.3. Binding site detection.

The SIRT6 protein's active site (PDBID: 3ZG6) was predicted using the SiteMap module in the Schrödinger suite (Schrödinger Release 2018-4: SiteMap, Schrödinger, LLC, New York, 2018). The SIRT6 protein's active binding site was predicted using default settings, with a minimum of 15 points per site. The site maps were then cropped to a distance of 4 Å from the nearest point on each site, resulting in the generation of four active binding sites [24].

2.1.4. Virtual screening.

Molecular docking techniques were employed to investigate the binding affinity of the flavonoid compounds with SIRT6. Pre-processed molecules were subjected to docking with SIRT6. The extra precision (XP) method of the Glide module was employed for docking with the active site determined using SiteMap. The output was formatted as a posture viewer file and then visualized using the Pose Viewer program. The docking methodology was validated by removing the molecule from the complex, re-docking, and determining the root mean square deviation (RMSD), which was found to be < 2 Å. [25].

2.2. Molecular mechanics generalized born surface area (MMGBSA).

The MM-GBSA module of Prime was used to compute the binding free energies of the ligand-receptor complexes. This module uses the XP dock pose viewer (PV) file as the input. The relative energies of the complexes were evaluated using the OPLS3 force field and VSGB solvation method. The binding free energies were computed using the equation proposed by Kollman [26,27].

$$\boldsymbol{G(binding\ affinity} = \mathbf{\Delta G\ (solvation\ enegy)} + \mathbf{\Delta E\ (minimized\ energy)} + \mathbf{\Delta G\ (surface\ area\ energies)} \quad (1)$$

2.3. ADMET analysis.

The ADMET properties of the selected ligands were assessed using two web servers: Swiss ADME (http://www.swissadme.ch/) and pkCSM (https://biosig.lab.uq.edu.au/pkcsm/) [23,28–30].

2.4. Molecular dynamics (MD) simulation.

The Desmond module within the Schrödinger suite was used to perform molecular dynamics (MD) simulations of the two most ADMET-favorable flavonoid compounds. The workflow consists of three successive steps: system builder, energy minimization, and molecular dynamics simulations[21,23]. The system was built using a single-point charge (SPC) solvent model with an orthorhombic bounding box. Subsequently, the model system was subjected to energy minimization. Simulations of related complexes were conducted using the NPT ensemble for a duration of 50 ns. TheNosé–Hoover thermostat algorithm and Martyna-Tobias-Klein barostat algorithm were used to ensure a constant pressure of 1 atm and a temperature of 300 K. The evaluation of short-range interactions involved the use of a cutoff value of 9.0 for coulombic interactions, as stated by John et al. (2015) [26,31–35].

The OPLS3 force field was chosen for docking and molecular dynamics simulations due to its broad applicability to proteins, ligands, and their complexes. It offers improved accuracy in predicting ligand conformations, binding poses, and interaction energies. Numerous prior studies on protein-ligand interactions have successfully employed OPLS3, and its compatibility with the Schrödinger suite further ensures the reliability of energetic and structural outputs in our system [21,36].

3. Results and Discussion

3.1. Virtual screening.

This study aimed to identify novel flavonoids with SIRT-6 modulatory action using *an in silico* approach. The 3D structure of SIRT6 was downloaded from the RCSB Protein Data Bank library and visualized (Figure 1A). Raw proteins were pre-processed using a protein preparation wizard (Figure 1B).

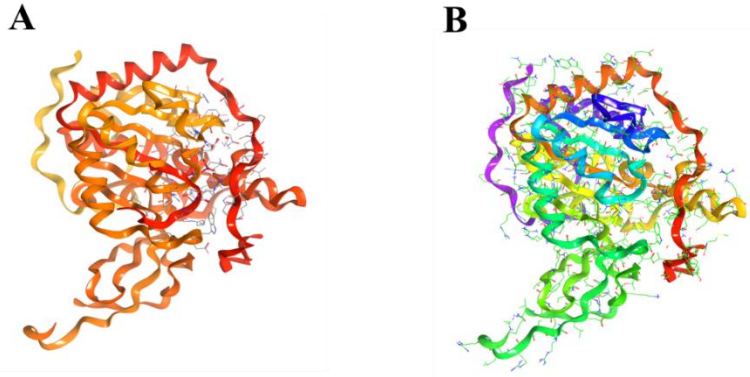

Figure 1. Structure of SIRT6 (3ZG6) **(A)** The raw structure of SIRT6 with a small-molecule activator retrieved from the protein data bank; **(B)** represents the pre-processed protein obtained following the protein preparation wizard.

The active site was identified using the SiteMap module, bundled with the Schrödinger Suite. Four top potential druggable pockets on the surface were identified (Figure 2).

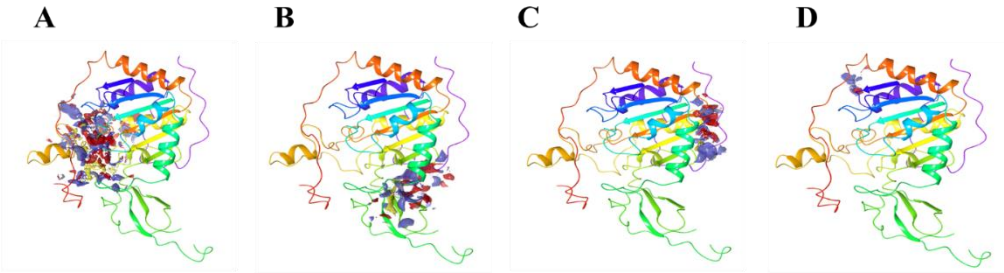

Figure 2. Active site detection using SiteMap. This figure shows the four best active sites obtained using the Schrödinger SiteMap module.

Site 1 had a drug score of ≈ 1, with a volume of 880.824 $Å^3$ (Table 1).

Table 1. Details of the best four active sites of SIRT6 using SiteMap.

Sites	Site score	Size	D Sore	Volume($Å^3$)
Site 1	1.068	437	1.032	880.824
Site 2	1.008	145	1.030	344.715
Site 3	0.716	51	0.677	148.176
Site 4	0.512	19	0.442	44.247

Based on the literature, site 1 is preferred for designing SIRT6 activators [15]. Hence, Site 1 was used for grid generation using the receptor grid generation wizard of the Schrödinger Suite.

In total, 239 flavonoids were included in this study. After successful docking, parameters such as docking score, ecoul (Coulomb energy) energy, Glide energy (Van Der Waals energy), Glide energy (Van Der Waals energy + Coulomb energy), and interacting residues (hydrogen bonds) with SIRT6 were assessed. The binding affinities of flavonoids to SIRT6 were analyzed and evaluated based on their docking scores. Out of the 239 compounds, more than 100 showed a docking score of <-5; however, the top 12 compounds were selected for further investigation (Table 2).

Table 2. Docking properties of selected compounds.

S.No.	Name	Glide rotatable bonds	Docking score	Glide evdw	Glide ecoul	Glide energy	Glide emodel	XP H bond	XP Lipophilic EvdW
1	Hibifolin	12	-14.04	-32.883	-17.669	-50.551	-57.587	-5.928	-3.012
2	Miquelianin	11	-13.481	-35.509	-14.498	-50.007	-60.673	-5.582	-2.757
3	Quercimeritrin	12	-12.941	-35.523	-20.284	-55.806	-74.028	-7.259	-3.253
4	1-Caffeoylquinic acid	10	-11.566	-34.492	-21	-55.492	-81.044	-4.998	-2.907
5	Isosilybin	9	-11.125	-48.751	-12.079	-60.83	-70.756	-4.607	-5.464
6	Baicalin	9	-11.087	-43.233	-16.731	-59.965	-77.326	-5.132	-3.643
7	Cynaroside	11	-11.065	-47.936	-16.015	-63.951	-93.696	-5.759	-4.032
8	Kaempferol 3-O-Î²-D-glucuronide	10	-10.933	-45.824	-13.953	-59.777	-57.836	-4.767	-3.354
9	Scutellarin	10	-10.769	-45.422	-13.076	-58.498	-87.697	-4.395	-3.774
10	Chrysin-7-O-glucuronide	8	-10.676	-46.442	-12.817	-59.259	-82.921	-4.035	-4.003
11	Astilbin	10	-10.515	-45.181	-12.991	-58.172	-85.943	-4.492	-3.616
12	Tilianin	10	-10.508	-46.021	-11.636	-57.657	-71.408	-5.279	-4.32

Docking score, including all additional terms: **Glide evdw**: Van der Waals energy; **Glide ecoul**: Coulomb energy; **Glide energy**: Modified Coulomb-van der Waals interaction energy; **Glide emodel:** Model energy, Emodel; **H Bond** H-bond pair term.

The 2D structure and docking pose of all 12 compounds showing the best docking results with SIRT6 are shown in Figure 3 and Figure 4, respectively.

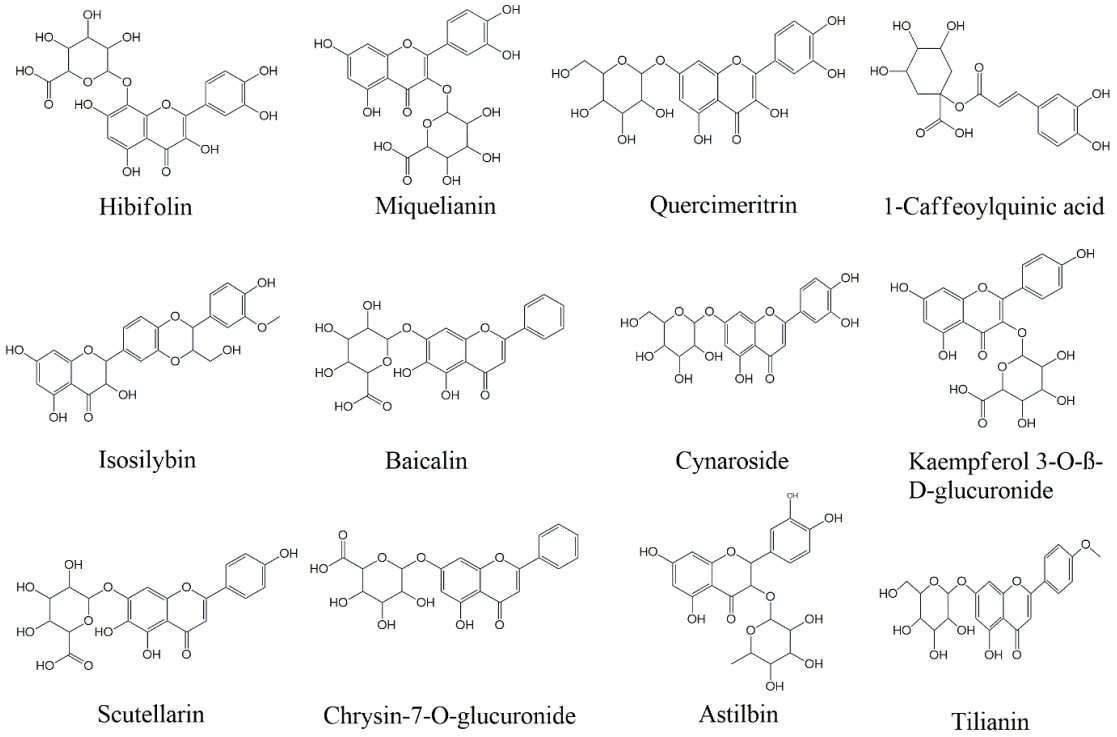

Figure 3. 2D structures of the compounds. The figure shows the 2D structure of the 12 compounds, showing the best docking result against SIRT6.

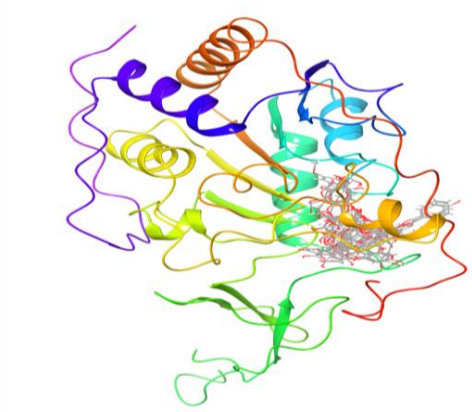

Figure 4. Dock poses of selected compounds. The figure represents the 3D docking pose of the best 12 docked compounds against SIRT6.

All 12 compounds, including Hibifolin, Miquelianin, Quercimeritrin, 1-Caffeoylquinic acid, Isosilybin, Baicalin, Cynaroside, Kaempferol 3-O-β-D-glucuronide, Scutellarin, Chrysin-7-O-glucuronide, Astilbin, Tilianin, Apigenin 7-glucoside, and (-)-Gallocatechin gallate exhibited docking scores between -10.25 and -14.04. The good binding affinities were due to good hydrogen binding, Coulomb energy, and van der Waals forces (Table 2). The 3D docking pose and 2D interaction revealed that GLN111, ARG63, TRP69, ASN2, PHE62, GLN111, SER8, ALA51, THR69, LEU184, ASP188, TRP186, ALA51, HID131, THR213, SER214, ILE217, ARG218, ARG218, ASP185, and LYS13 in chain A played important roles in ligand binding. (Figures 5,6, Table 3).

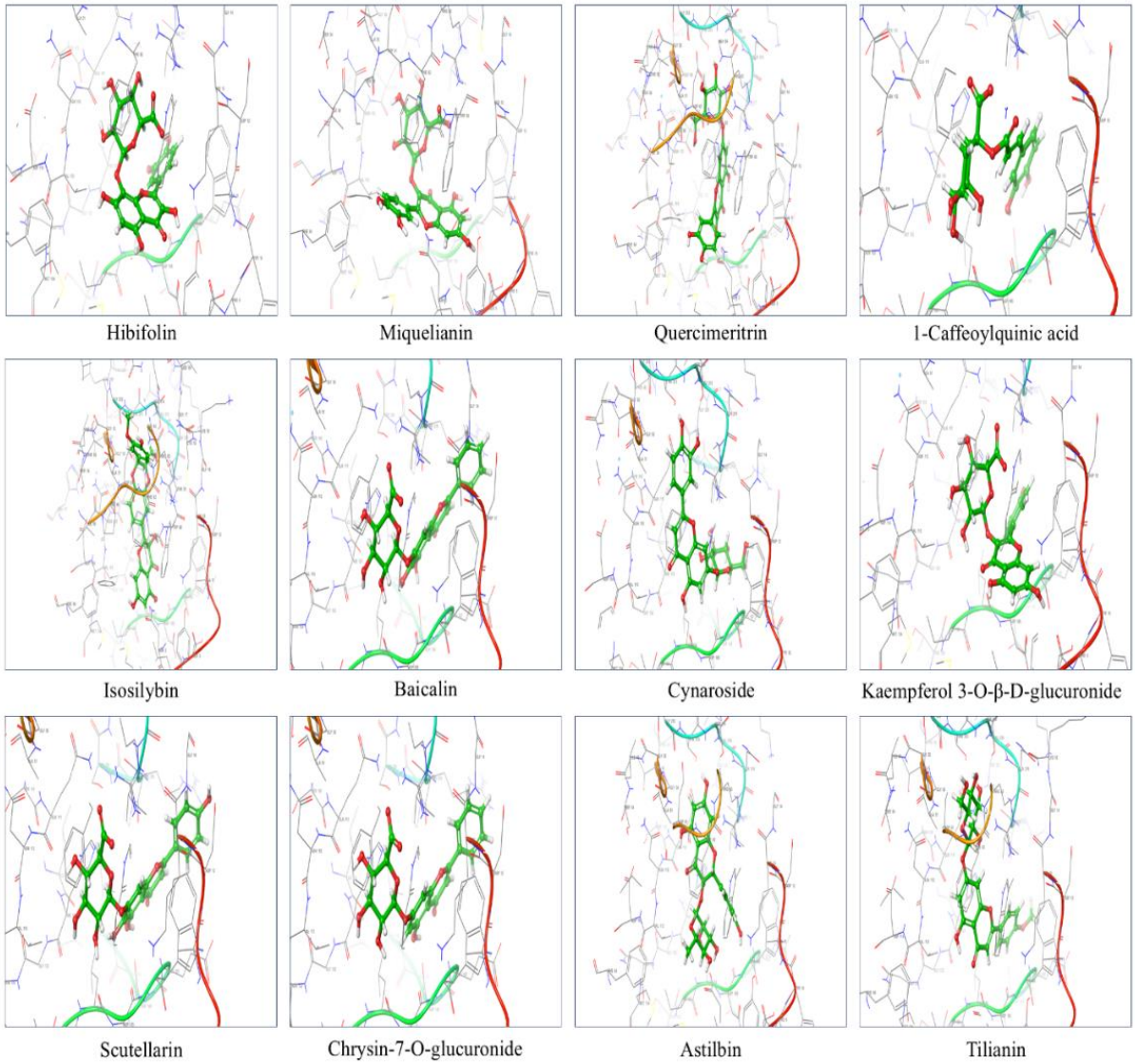

Figure 5. 3D docking pose of the top 12 compounds docked with SIRT6. The output of the Schrödinger 3D diagram shows the binding site residues of SIRT6 with the top 12 docked compounds.

Table 3. List of top identified molecules with different types of interactions with active site residues (PDB 3ZG6).

S.No.	Name	# Contacts		Active Site Residues
		HB	π- π	
1	Hibifolin	5	3	GLN111, ARG63, TRP69, ASN2, PHE62
2	Miquelianin	5	3	GLN111, TRP69, SER8, ASN2, ARG63, PHE62
3	Quercimeritrin	7	2	ALA51, THR69, SER8, ASN2, ARG63, PHE62, GLN111, LEU184
4	1-Caffeoylquinic acid	6	1	ASP188, ARG63, TRP69, LEU184, TRP186
5	Isosilybin	4	1	ARG63, GLN111, ALA51, LEU184, HID131
6	Baicalin	4	1	TRP69, ARG63, LEU184, TRP186, ASP188
7	Cynaroside	5	0	THR213, SER214, ILE217, ARG218, LEU184
8	Kaempferol 3-O-Î²-D-glucuronide	3	1	ARG63, TRP69, SER8
9	Scutellarin	5	1	HID131, TRP69, ARG63, LEU184, TRP186, ASP188
10	Chrysin-7-O-glucuronide	5	1	HID131, ARG63, LEU184, TRP69, TRP186, ASP188
11	Astilbin	4	0	THR213, ALA51, LEU184
12	Tilianin	2	1	ALA51, SER214, PHE62

HB No of hydrogen bond; **π-π** No of pi-pi stacking.

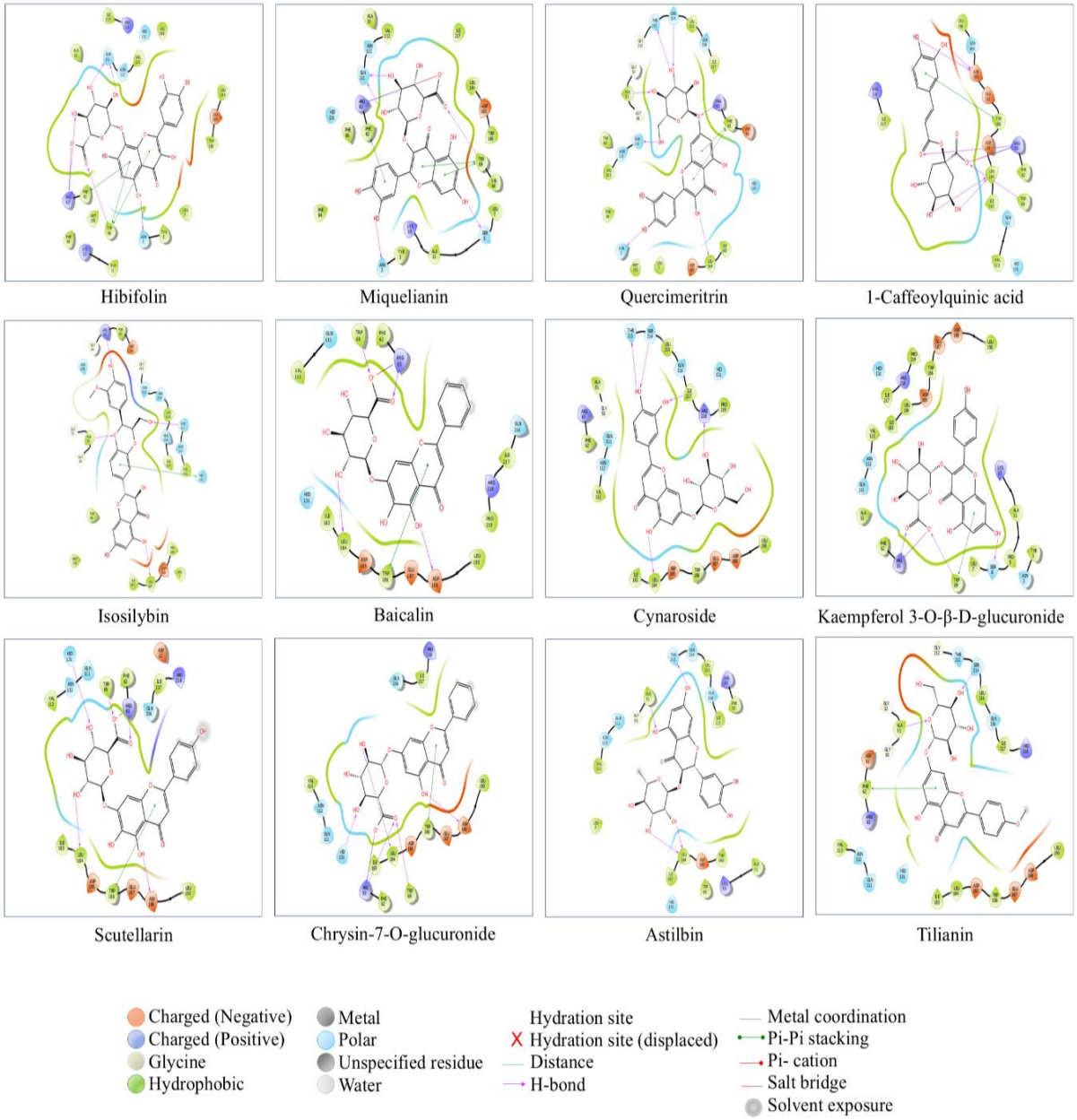

Figure 6. 2D interaction of the top 12 compounds docked with SIRT6. Output of Schrödinger 2D interaction diagram of SIRT6 with top docked compounds.

Hibifolin is a flavanol glycoside isolated from herbal medicines, e.g., Abelmoschus Manihot and Melochia corchorifolia [37]. Hibifolin has a strong neuroprotective effect but no estrogenic effects [37,38]. The docking score for hibifolin was found to be -14.04. The docking score was attributed to 5 hydrogen bond formations between hibifolin and SIRT-6 at Glutamine, Arginine, Tryptophan, Asparagine, and Phenylalanine (Fig. 5-6). Miquelianin, a natural flavonoid, is a metabolite derived from quercetin. Miquelianin inhibits CBR1 [39]. The docking score for miquelianin was observed to be -13.481. The docking score was attributed to 5 hydrogen bonds at Glutamine, Tryptophan, Serine, Asparagine, Arginine, and Phenylalanine (Figures 5,6, Table 3). Quercimeritrin is an α-glucosidase-selective inhibitor [40]. The docking score for quercitrin was -12.941. The docking score was attributed to 7 hydrogen bonds at Alanine, Threonine, Serine, Asparagine, Arginine, Phenylalanine, Glutamine, Leucine, along with good Van der Waals energy (Figures 5,6, Tables 2, 3). 1-Caffeoylquinic acid is a potent inhibitor of NF-κB, demonstrating a strong affinity for the RH domain of p105 with a Ki value of 0.002 μM and a binding energy of 1.50 Kcal/mol.

Caffeoylquinic acid exhibits antioxidant properties against oxidative stress. 1-Caffeoylquinic acid hinders the interaction between PD-1 and PD-L1 [41]. The docking score for 1-Caffeoylquinic acid was found to be -11.566. The docking score was attributed to 6 hydrogen bonds with Asparagine, Arginine, Tryptophan, Leucine, and good van der Waals energy (Fig. 5-6, Table 2-3). Isosilybin is a novel inhibitor of PXR-mediated CYP3A4 induction. Isosilybin could be considered a potential option for developing highly effective PXR antagonists to mitigate drug-drug interactions mediated by CYP3A4 in cancer patients [42]. The docking score for isosilybin was -11.125. The docking score was attributed to 4 hydrogen bonds between isosilybin and SIRT6 at Arginine, Glutamine, Alanine, Leucine, and histidine (Figures 5,6, Tables 2-3). Baicalin is an allosteric carnitine palmityl transferase 1 (CPT1) activator [43]. The docking score for baicalin was observed to be -11.087. The docking score was attributed to 4 hydrogen bonds along with one π–π stacking (Figures 5,6, Tables 2-3). Cynaroside has antioxidant properties. Additionally, it is a potent inhibitor of influenza RNA-dependent RNA polymerase [44]. The docking score for Cynaroside was -11.065. The docking score was attributed to 5 hydrogen bonds along with 0 pi-pi stacking (Figures 5,6, Tables 2-3). Kaempferol 3-O-β-D-glucuronide (Kaempferol-3-glucuronide) is an anti-inflammatory form of kaempferol. Kaempferol 3-O-β-D-glucuronide substantially reduces pro-inflammatory mediators, such as IL-1β, NO, PGE2, and LTB4 [45]. Kaempferol reduces inflammation by increasing the release of the anti-inflammatory cytokine IL-10. The docking score for Cynaroside was -11.065. The docking score was attributed to 3 hydrogen bonds along with one π–π stacking (Figures 5, 6; Tables 2, 3). Scutellarin is a glycosyloxyflavone and a 7-O-glucuronide of scutellarin. It functions as both an antineoplastic agent and a proteasome inhibitor [46]. This compound is a glycosyloxyflavone, glucosiduronic acid, trihydroxyflavone, and a monosaccharide derivative. It has a functional relationship with scutellarein. It functions as a conjugate acid of scutellarin (1-). The docking score for Cynaroside was -10.769. The docking score was attributed to five hydrogen bonds along with one π–π stacking (Figures 5,6, Tables 2-3). Chrysin-7-O-glucuronide is a flavonoid extracted from Scutellaria baicalensis that has antioxidant activity. The docking score for Chrysin-7-O-glucuronide was -10.676, attributed to five hydrogen bonds along with 1 pi-pi stacking (Fig. 5-6, Table 2,3). Astilbin is a compound that promotes the activation of NRF2. Astilbin further inhibits TNF-α production and NF-κB activation [47]. The docking score for Chrysin-7-O-glucuronide was -10.515, which was attributed to four hydrogen bonds along with 0 pi-pi stacking (Figures 5,6, Tables 2-3). Tilianin is a flavonoid glycoside found in various medicinal plants. It hinders the activation of NF-κB and the activation, phosphorylation, and destruction of IkB kinase [48]. The docking score of tilianin was observed to be -10.508. The docking score was attributed to two hydrogen bonds between tilianin and SIRT6 at alanine, serine, and 1 pi-pi interaction with phenylalanine (Figures 5,6, Tables 2-3). Apigenin 7-glucoside, also known as Apigenin-7-O-β-D-glucopyranoside, has notable anti-proliferative properties and acts as an antioxidant by scavenging reactive oxygen species (ROS). The docking score for apigenin 7-glucoside was -10.406, which was attributed to five hydrogen bonds along with 1 pi-pi stacking (Figures 5,6, Tables 2-3). (-) - Gallocatechin gallate is a potent inhibitor of ABA-induced stomatal closure. The docking score for (-) - Gallocatechin Gallate was -10.255, which was attributed to four hydrogen bonds along with two π-π stacking (Figures 5, 6; Tables 2, 3).

3.2. Absorption, distribution, metabolism, excretion, and toxicity (ADMET) screening of the top 12 flavonoids.

The efficacy of a drug candidate is influenced not only by its potency but also by its favorable ADMET profile. Various ADMET techniques are available that anticipate the critical properties of molecules using computer simulations, which are useful for examining their key qualities. Currently, it is recommended to utilize computational ADMET in the initial phase of drug development, alongside *in vivo* and *in vitro* research, to minimize safety issues. The present study utilized freely available Internet web servers, namely SwissADME [49] and pkCSM, to conduct ADMET profiling [30]. According to the ADMET analysis, none of the selected compounds had the ability to cross the blood-brain barrier (BBB). Furthermore, most compounds lacked inhibitory activity against cytochrome P450 isomers, namely, CYP2C9. CYP2C9 is a significant cytochrome P450 enzyme that plays a crucial role in the metabolism of several drugs, such as NSAIDs, oral anticoagulants, and oral hypoglycemics. When CYP2C9 activity is inhibited, the metabolism of the aforementioned drugs is reduced, increasing their concentration in the blood. This can result in severe adverse effects. Therefore, the absence of CYP2C9 inhibitory activity indicates a minimal likelihood of medication interactions through the CYP2C9 metabolic pathway, as shown in Table 4.

The pharmacokinetics and pharmacodynamics of a drug are influenced by its molecular weight (MW). Optimal passive diffusion across cell membranes typically occurs when the molecular weight is below 500 g/mol. Small molecules can penetrate the cell membranes and travel through tissues to reach their intended targets. In contrast, larger molecules face challenges, such as poor absorption and restricted membrane permeability, leading to lower bioavailability. Larger molecules often require carriers for effective distribution to ensure they reach their intended target. The molecular weight also influences drug metabolism and excretion, with small molecules being metabolized and excreted more rapidly than larger molecules. Moreover, larger molecules typically exhibit increased toxicity as they accumulate within the body and possess longer half-lives. In this study, a threshold of 500 g/mol was used (Table 4). In this study, the acceptable range for molar refractivity (MR), an indicator of compound polarity, was set between 40 and 130. The top 12 compounds had MRs that were within this range (Table 4). The aqueous solubility of a compound plays a crucial role in its absorption and distribution properties. The water solubility (log S) of a substance indicates its solubility in water at 25°C and serves as a measure of compound solubility.

Compounds that are soluble in lipids are typically absorbed less effectively than those that are soluble in water, particularly when administered orally. In this regard, the log S value determined using the ESOL model should ideally be 6. All 12 compounds were soluble in water, except for isosilybin, which showed moderate solubility with a Log S value of -4.14. Lipinski's Rule of Five (ROF) serves as a guideline for the oral activity of compounds, stating that an orally active drug should not break more than one of the following rules: having a number of hydrogen bond acceptors less than or equal to 10, a number of hydrogen bond donors less than or equal to 5, a molecular weight less than 500 Daltons, and an octanol-water partition coefficient (LogP) less than or equal to 5. None of the 12 selected compounds showed more than one violation. Synthetic Accessibility (SA) scores are derived from the concept that the occurrence frequency of molecular fragments in readily accessible molecules corresponds to ease of synthesis. SA scores varied between 1 (indicating ease) and 10 (indicating extreme difficulty). All the compounds exhibited SA scores exceeding 4.0.

Moreover, orally administered drugs are absorbed through the gastrointestinal system, and the extent of their absorption in the intestine can affect their bioavailability. The pKCM web server showcased that the majority of the flavonoids analyzed exhibited intestinal absorption rates exceeding 30%, with the exceptions being Hibifolin, Miquelianin, Baicalin, Kaempferol 3-O-β-D-glucuronide, Scutellarin, and Chrysin-7-O-glucuronide as listed in Table 5. Achieving effective skin permeability and sensitivity is crucial for the success of various drugs and is a key focus in the development of transdermal drug delivery systems. The skin permeability constant, represented by the logKp value (cm/h), serves as a vital parameter for evaluating skin permeability. If a substance exhibited a logKp value greater than -2.5, it was classified as having poor skin permeability. Analysis conducted through the pkCSM web server revealed that the top 12 ranked compounds had logKp values below -2.5, indicating their ability to effectively penetrate the skin. Cardiac toxicity is a significant factor that prompts withdrawal in drug discovery and is chiefly attributed to drug interactions with the human ether-a-go-go-related (hERG) gene-encoded cardiac potassium channel. This interaction can result in long QT syndrome and, ultimately, sudden death (Lee et al., 2019). According to pkCSM analysis, none of the 12 compounds displayed the ability to inhibit hERG I (see Table 5). The *in silico* Ames toxicity test uses computer-based methods to assess the mutagenic properties of compounds using predictive models. Analysis using pkCSM indicated that none of the selected compounds were likely to induce AMES toxicity.OCT-2 (Organic Cation Transporter 2) plays a crucial role as a renal uptake transporter, facilitating the clearance and elimination of drugs and endogenous compounds. Concurrent administration of OCT-2 inhibitors and substrates can lead to adverse drug interactions. Therefore, understanding whether a drug candidate can be transported by OCT-2 is vital in drug discovery, as it offers insights into drug clearance mechanisms and potential side effects. In the current investigation, ADMET profiling revealed that none of the selected compounds could be transported by OCT-2. Hence, thorough ADMET profiling carried out via SwissADME and pkCSM indicated that out of the selected compounds, only Isosilybin and Tilianin demonstrated favorable drug-like attributes. Consequently, only these two compounds were subjected to further analysis (Table 5).

Table 4. ADMET properties of selected compounds using SwissADME.

S. No.	Name	Mol. Weight	No. of heavy atoms	Molar refractivity	CYP2C9 inhibitor	BBB permeant	Log S (ESOL)	Sol. class	No. of Lipinski violations	Synthetic accessibility
1	Hibifolin	494.36	35	112.79	No	No	-3.14	S	2	5.48
2	Miquelianin	478.36	34	110.77	No	No	-3.27	S	2	5.26
3	Quercimeritrin	464.38	33	110.16	No	No	-3.04	S	2	5.31
4	1-Caffeoylquinic acid	3.54.31	25	83.50	No	No	-1.62	S	1	4.15
5	Isosilybin	482.44	35	120.55	No	No	-4.14	MS	0	4.92
6	Baicalin	446.36	32	106.72	No	No	-3.41	S	2	5.09
7	Cynaroside	448.38	32	108.13	No	No	-3.65	S	2	5.17
8	Kaempferol 3-O-β-D-glucuronide	462.36	33	108.74	No	No	-3.41	S	1	5.22
9	Scutellarin	462.36	33	108.74	No	No	-3.27	S	2	5.12
10	Chrysin-7-O-glucuronide	430.36	31	104.70	No	No	-3.55	S	0	5.03
11	Astilbin	450.39	32	105.98	No	No	-2.62	S	2	5.27
12	Tilianin	446.40	32	110.58	No	No	-4.00	S	0	5.23

S: Soluble; **MS**: Moderately soluble.

Table 5. ADMET properties of selected compounds using pkCSM.

S. No	Name	Mol. weight	No of rot. bond	Intestinal absorption (Human)	Skin permeability	hERG I inhibitor	AMES toxicity	Renal OCT2 substrate	Oral Rat acute toxicity (LD50)	Oral Rat chronic toxicity (LOAEL)	Skin sensation	Hepatotoxicity
1	Hibifolin	494.36	4	6.603	-2.735	No	No	No	2.491	4.477	No	No
2	Miquelianin	478.36	4	25.112	-2.735	No	No	No	2.497	4.51	No	No
3	Quercimeritrin	464.38	4	33.633	-2.735	No	No	No	2.543	4.162	No	No
4	1-Caffeoylquinic acid	354.31	4	31.578	-2.735	No	No	No	2.001	2.795	No	No
5	Isosilybin	482.44	4	69.767	-2.735	No	No	No	2.557	3.514	No	No
6	Baicalin	446.36	4	26.224	-2.735	No	No	No	2.634	4.536	No	No
7	Cynaroside	448.38	4	37.556	-2.735	No	No	No	2.547	4.279	No	No
8	Kaempferol 3-O-β-D-glucuronide	462.36	4	25.165	-2.735	No	No	No	2.513	4.641	No	No
9	Scutellarin	462.36	4	13.836	-2.735	No	No	No	2.538	4.503	No	No
10	Chrysin-7-O-glucuronide	430.36	4	25.474	-2.735	No	No	No	2.744	4.574	No	No
11	Astilbin	450.39	3	49.005	-2.735	No	No	No	2.589	3.354	No	No
12	Tilianin	446.40	5	46.529	-2.735	No	No	No	2.72	4.436	No	No

3.3. MMGBSA analysis.

To validate the accuracy, the Glide docking poses of the isosilybin and tiilianin SIRT6 complexes were evaluated using MM-GBSA, which has been shown to better discriminate between true and decoy ligand poses and determine the energetically preferred positions. The ΔG_{bind} values for Isosilybin and Tilianin were observed to be -82.43 and -92.12, respectively (Table 6).

Table 6. Binding free energy calculation of two top docked ADMET favourable compounds using the Prime/MM-GBSA approach.

S.N.	Name	ΔG bind	ΔG bind coulomb	ΔG bind lipophilic	ΔG bind solv GB	ΔG bind vdW
1	Isosilybin	-82.43	-20.75	-51.73	31.06	-52.21
2	Tilianin	-92.12	-29.74	-47.26	30.81	-48.75

Coulomb—Coulomb energy; **Hbond**—Hydrogen-bonding correction; **Lipo**—Lipophilic energy; **Solv GB**—Generalized Born electrostatic solvation energy; **vdW**—Van der Waals

3.4. Molecular dynamics simulations of best docking poses.

Molecular docking was employed to predict the mechanisms of protein/ligand interactions; however, it was unable to predict the stability and dynamic behavior of the molecules throughout the binding process. Developing comprehension through experimentation is also a time-consuming process. However, the occurrence of troublesome molecular behavior can be predicted by simulating molecular activity inside a computer framework [34,50]. The complexes of Isosilybin and Tilianin, with SIRT6, acquired through molecular docking, were validated by subjecting them to 50ns MD simulations [51–54].

Molecular dynamics experiments of Isosilybin and Tilianin provide comprehensive insights into the stability of ligand-protein complexes under different solvent conditions. Root-mean-square deviation (RMSD) values were used to assess the relative alterations in atom displacements compared with a reference frame. A system was considered equilibrated and stabilized when it exhibited consistently low RMSD levels and uniform variations throughout the simulation. However, the stability was indicated by significant fluctuations. RMSDs of approximately 1–3 Å were ideal for small proteins. In a realistic aqueous setting, MD simulations showed that the MDL800 SIRT6 interactions were stable. Our findings of acceptable protein RMSD levels are in line with those of a previous study [55]. Throughout the 50ns simulation of the isosilybin-SIRT6 complex, the SIRT6 RMSD changes were within the specified range (0.9 Å to 3.1 Å), while the Isosilybin RMSD values ranged from 1.25 Å to 2.5 Å, demonstrating high binding stability (Figure 7A). Throughout the 50ns simulation of the Tilianin -SIRT6 complex, the fluctuations in RMSD of SIRT6 remained within the specified range of .2.1Å to 5.2 Å. The RMSD values of Tilianin ranged from 0.9 Å to 3.4 Å, showing a favorable level of binding stability (Figure 7B).

Protein Root Mean Square Fluctuation (P-RMSF) is a useful measure for describing small-scale variations within protein chains. MD simulation investigations of Isosilybin and Tilianin-SIRT6 complexes revealed that only a few amino acids exhibited a P-RMSF greater than 3.5 Å. (Figures 8A–D) Conversely, ligand root-mean-square fluctuation (L-RMSF) is valuable for analyzing alterations in the locations of the ligand atoms. MD investigations of the corresponding complexes revealed that only a few atoms exhibit high L-RMSF values. Moreover, the analysis of protein-ligand interactions conducted over a duration of 50ns indicated that isosilybin and tiilianin established robust hydrogen bonds with SIRT6 during

molecular dynamic simulations (Figure 7C-D). The stability of SIRT6-Isosilybin and Tilianin complexes was confirmed using protein RMSDs, P-RMSFs, protein interaction analysis, and L-RMSFs throughout a 50 ns MD simulation [56].

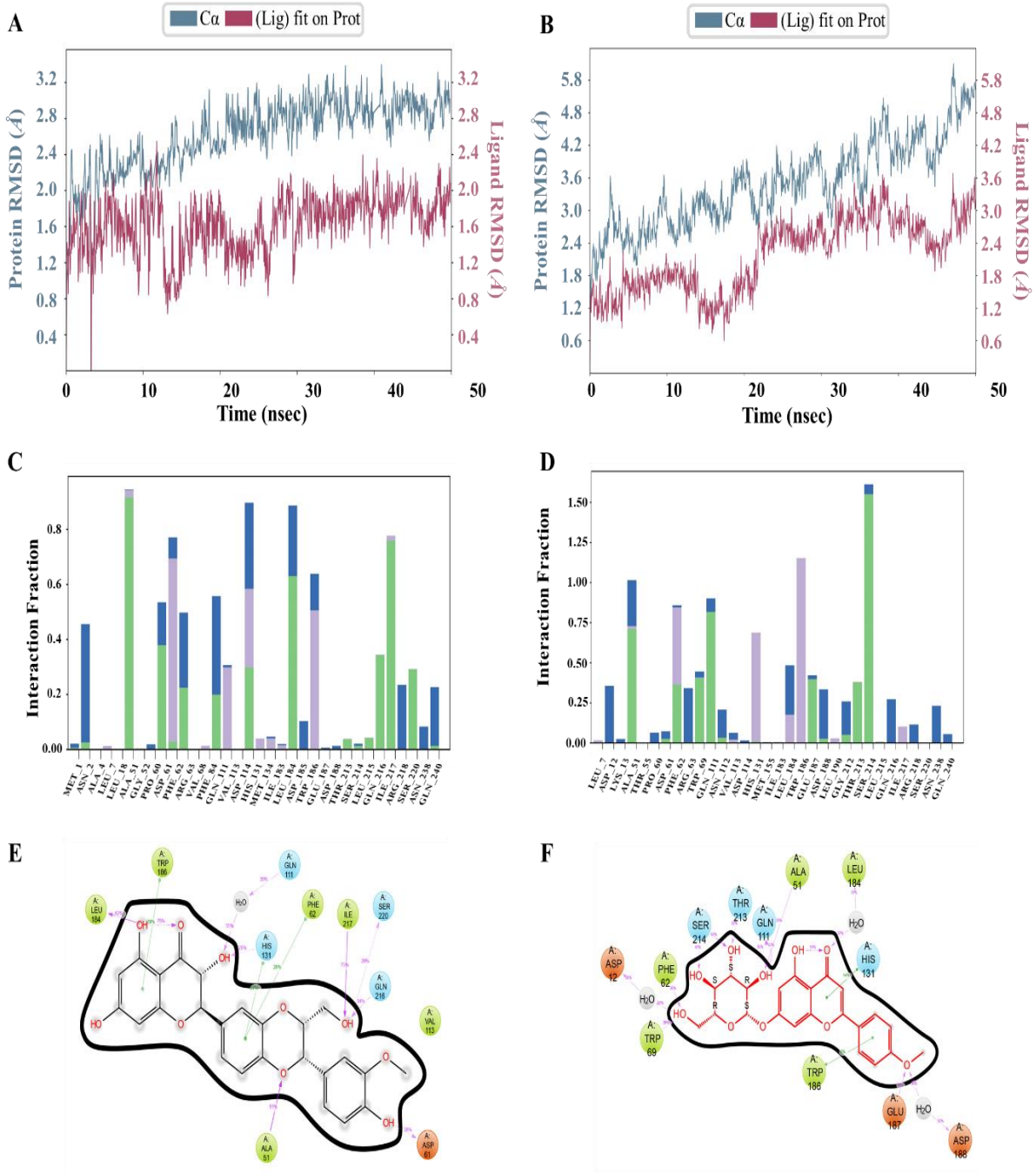

Figure 7. RMSD, protein interaction, and protein-ligand contacts of top docked ADMET favorable flavonoid compounds **(A-B)** RMSD; **(C-D)** protein interaction; **(E-F)** protein-ligand contacts plot of Isosylibin and tilianin over simulations run for 50ns complexed with SIRT6, respectively.

Literature reports indicate that quercetin, a known SIRT6 activator, exhibits ΔG_{bind} values ranging from approximately -22.8 kcal/mol under comparable simulation conditions [57]. In our study, Isosilybin and Tilianin demonstrated ΔG_{bind} values of –82.43 and –92.12 kcal/mol, respectively, placing them within a similar or even superior range. Molecular dynamics simulations further supported these findings, revealing consistent RMSD values and stable hydrogen bonding interactions for both flavonoid SIRT6 complexes. These observations suggest that Isosilybin and Tilianin possess binding affinity and complex stability comparable to established synthetic activators, highlighting their promise as natural alternatives for SIRT6

modulation. Nevertheless, while this study presents Isosilybin and Tilianin as newly identified SIRT6 activators, it is important to acknowledge certain limitations.. Initially, a molecular dynamics simulation lasting 50 ns was performed exclusively for Isosilybin and Tilianin, which had the highest docking scores and excellent ADMET properties.

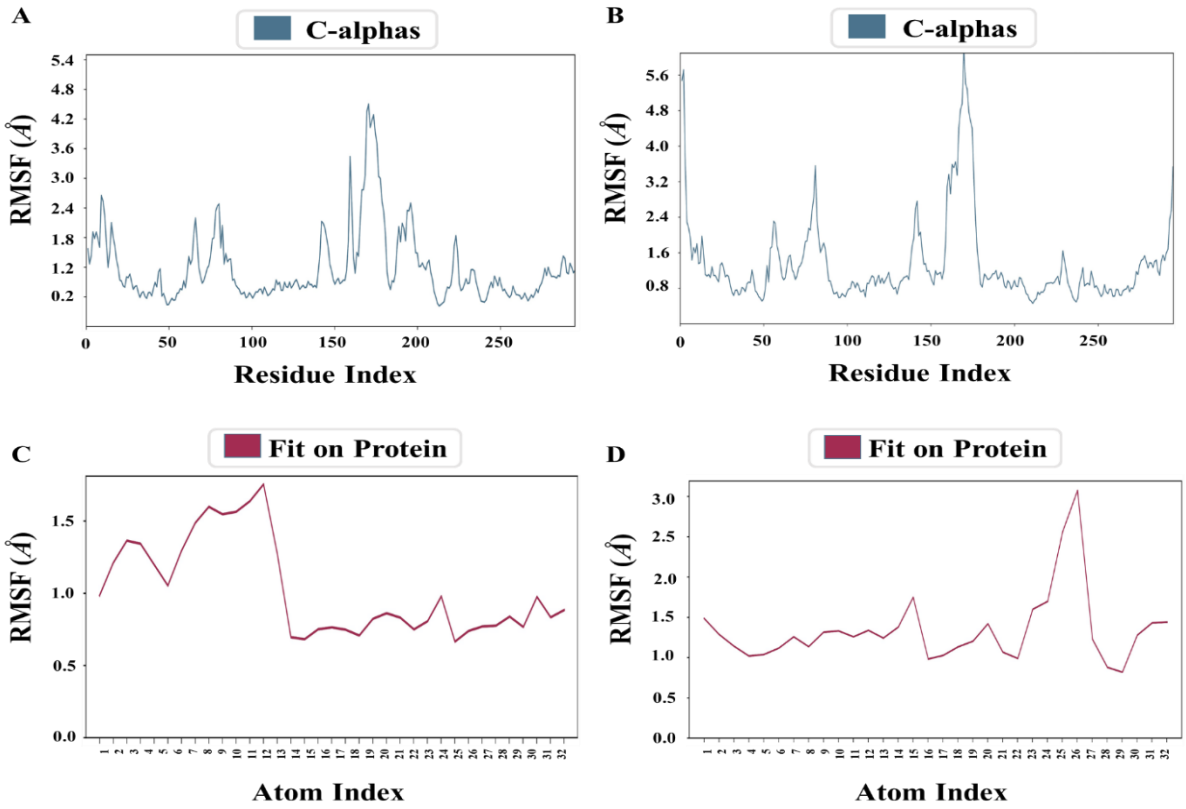

Figure 8. RMSF of top docked ADMET-favorable flavonoid compounds (A-B) RMSF residue index, (C-D) RMSF atom index of isosylibin and tilianin over simulations run for 50ns complexed with SIRT6

In addition, MMGBSA was performed using the Glide docking poses of the Isosilybin and Tilianin-SIRT6 complexes to evaluate their static behavior. Molecular dynamics simulations lasting 50 ns were conducted to investigate the dynamic behavior of the protein-ligand complexes. This study was purely theoretical and relied exclusively on computational techniques and simulations. Although these techniques offer valuable insights and predictions, further validation is required through extensive *in vitro* and *in vivo* investigations.

4. Conclusion

Reduced SIRT6 expression is linked to a number of chronic diseases, such as aging, diabetes, and cardiovascular disease. The current study involved screening 239 flavonoid compounds for their ability to bind with SIRT6 using Glide module of Schrödinger. Out of all the compounds, the top 12 were chosen based on their docking scores. Further analysis of their ADMET profiles showed that two of the 12 compounds, Isosilybin and Tilianin, had favorable drug-like qualities. Furthermore, the utilization of MMGBSA and molecular dynamics investigations demonstrated that Isosilybin and Tilianin could form stable complexes with SIRT6 in solvents. This study elucidated the ability of several flavonoid compounds to function as SIRT6 activators and identified Isosilybin and Tilianin as possible SIRT6 activators.

Author Contributions

Writing—original draft preparation, A.S.K.; investigation, A.S.K.; validation, V.A.; formal analysis, M.R., R.C., S.S., A.M., V.M.; supervision, V.M.; project administration, V.M.; writing—review and editing, V.M. All authors have read and agreed to the published version of the manuscript..

Institutional Review Board Statement

Not applicable.

Informed Consent Statement

Not applicable.

Data Availability Statement

The data of this study will be available from the corresponding author upon reasonable request.

Funding

This work was supported by the ICMR Senior Research Fellowship (File No. **3/1/2(05)/OBS/2022-NCD-II**) awarded to Arjun Singh Kaushik.

Acknowledgement

We acknowledge the Indian Council of Medical Research for supporting this research.

Conflict of Interest

The authors declare that this research was conducted in the absence of any commercial or financial relationships that could be construed as a potential conflict of interest.

References

1. Wu, Q.-J.; Zhang, T.-N.; Chen, H.-H.; Yu, X.-F.; Lv, J.-L.; Liu, Y.-Y.; Liu, Y.-S.; Zheng, G.; Zhao, J.-Q.; Wei, Y.-F.; Guo, J.-Y.; Liu, F.-H.; Chang, Q.; Zhang, Y.-X.; Liu, C.-G.; Zhao, Y.-H. The sirtuin family in health and disease. *Signal Transduct. Target. Ther.* **2022**, *7*, 402, https://doi.org/10.1038/s41392-022-01257-8.
2. Carafa, V.; Rotili, D.; Forgione, M.; Cuomo, F.; Serretiello, E.; Hailu, G.S.; Jarho, E.; Lahtela-Kakkonen, M.; Mai, A.; Altucci, L. Sirtuin functions and modulation: from chemistry to the clinic. *Clin. Epigenetics* **2016**, *8*, 61, https://doi.org/10.1186/s13148-016-0224-3.
3. Vachharajani, V.; McCall, C.E. Sirtuins: potential therapeutic targets for regulating acute inflammatory response?. *Expert Opin. Ther. Targets* **2020**, *24*, 489–497, https://doi.org/10.1080/14728222.2020.1743268.
4. Sanders, B.D.; Jackson, B.; Marmorstein, R. Structural basis for sirtuin function: What we know and what we don't. *Biochim. Biophys. Acta - Proteins Proteom.* **2010**, *1804*, 1604–1616, https://doi.org/10.1016/j.bbapap.2009.09.009.
5. Poltronieri, P.; Čerekovic, N. Roles of Nicotinamide Adenine Dinucleotide (NAD^+) in Biological Systems. *Challenges* **2018**, *9*, 3, https://doi.org/10.3390/challe9010003.
6. Divya, K.P.; Kanwar, N.; Anuranjana, P.V.; Kumar, G.; Beegum, F.; George, K.T.; Kumar, N.; Nandakumar, K.; Kanwal, A. SIRT6 in Regulation of Mitochondrial Damage and Associated Cardiac Dysfunctions: A Possible Therapeutic Target for CVDs. *Cardiovasc. Toxicol.* **2024**, *24*, 598-621, https://doi.org/10.1007/s12012-024-09858-1.

7. Fiorentino, F.; Mai, A.; Rotili, D. Emerging Therapeutic Potential of SIRT6 Modulators. *J. Med. Chem.* **2021**, *64*, 9732–9758, https://doi.org/10.1021/acs.jmedchem.1c00601.
8. Pan, P.W.; Feldman, J.L.; Devries, M.K.; Dong, A.; Edwards, A.M.; Denu, J.M. Structure and Biochemical Functions of SIRT6*. *J. Biol. Chem.* **2011**, *286*, 14575–14587, https://doi.org/10.1074/jbc.M111.218990.
9. Jiang, H.; Khan, S.; Wang, Y.; Charron, G.; He, B.; Sebastian, C.; Du, J.; Kim, R.; Ge, E.; Mostoslavsky, R.; Hang, H.C.; Hao, Q.; Lin, H. SIRT6 regulates TNF-α secretion through hydrolysis of long-chain fatty acyl lysine. *Nature* **2013**, *496*, 110-113, https://doi.org/10.1038/nature12038.
10. Cardinale, A.; de Stefano, M.C.; Mollinari, C.; Racaniello, M.; Garaci, E.; Merlo, D. Biochemical Characterization of Sirtuin 6 in the Brain and Its Involvement in Oxidative Stress Response. *Neurochem. Res.* **2015**, *40*, 59-69, https://doi.org/10.1007/s11064-014-1465-1.
11. Garcia-Venzor, A.; Toiber, D. SIRT6 Through the Brain Evolution, Development, and Aging. *Front. Aging Neurosci.* **2021**, *13*, 747989, https://doi.org/10.3389/fnagi.2021.747989.
12. Kaluski, S.; Portillo, M.; Besnard, A.; Stein, D.; Einav, M.; Zhong, L.; Ueberham, U.; Arendt, T.; Mostoslavsky, R.; Sahay, A.; Toiber, D. Neuroprotective Functions for the Histone Deacetylase SIRT6. *Cell Rep.* **2017**, *18*, 3052-3062, https://doi.org/10.1016/j.celrep.2017.03.008.
13. Michishita, E.; McCord, R.A.; Berber, E.; Kioi, M.; Padilla-Nash, H.; Damian, M.; Cheung, P.; Kusumoto, R.; Kawahara, T.L.A.; Barrett, J.C.; Chang, H.Y.; Bohr, V.A.; Ried, T.; Gozani, O.; Chua, K.F. SIRT6 is a histone H3 lysine 9 deacetylase that modulates telomeric chromatin. *Nature* **2008**, *452*, 492-496, https://doi.org/10.1038/nature06736.
14. Chen, P.-T.; Yeong, K.Y. New sirtuin modulators: their uncovering, pharmacophore, and implications in drug discovery. *Med. Chem. Res.* **2024**, *33*, 1064–1078, https://doi.org/10.1007/s00044-024-03249-5.
15. Klein, M.A.; Denu, J.M. Biological and catalytic functions of sirtuin 6 as targets for small-molecule modulators. *J. Biol. Chem.* **2020**, *295*, 11021–11041, https://doi.org/10.1074/jbc.REV120.011438.
16. Guo, Z.; Li, P.; Ge, J.; Li, H. SIRT6 in Aging, Metabolism, Inflammation and Cardiovascular Diseases. *Aging Dis.* **2022**, *13*, 1787–1822, https://doi.org/10.14336/AD.2022.0413.
17. Shang, J.L.; Ning, S.B.; Chen Y.Y.; Chen T.X.; Zhang J. MDL-800, an allosteric activator of SIRT6, suppresses proliferation and enhances EGFR-TKIs therapy in non-small cell lung cancer. *Acta Pharmacol Sin*. 2021;42(1):120-131. doi:10.1038/s41401-020-0442-2
18. Zhang, J.; Li, Y.; Liu, Q.; Huang, Y.; Li, R.; Wu, T.; Zhang, Z.; Zhou, J.; Huang, H.; Tang, Q.; Huang, C.; Zhao, Y.; Zhang, G.; Jiang, W.; Mo, L.; Zhang, J.; Xie, W.; He, J. Sirt6 Alleviated Liver Fibrosis by Deacetylating Conserved Lysine 54 on Smad2 in Hepatic Stellate Cells. *Hepatology* **2021**, *73*, 1140–1157, https://doi.org/10.1002/hep.31418.
19. Iachettini, S.; Trisciuoglio, D.; Rotili, D.; Lucidi, A.; Salvati, E.; Zizza, P.; Di Leo, L.; Del Bufalo, D.; Ciriolo, M.R.; Leonetti, C.; Steegborn, C.; Mai, A.; Rizzo, A.; Biroccio, A. Pharmacological activation of SIRT6 triggers lethal autophagy in human cancer cells. *Cell Death Dis.* **2018**, *9*, 996, https://doi.org/10.1038/s41419-018-1065-0.
20. Lu, S.; Chen, Y.; Wei, J.; Zhao, M.; Ni, D.; He, X.; Zhang, J. Mechanism of allosteric activation of SIRT6 revealed by the action of rationally designed activators. *Acta Pharm. Sin. B* **2021**, *11*, 1355-1361, https://doi.org/10.1016/j.apsb.2020.09.010.
21. Agarwal, V.; Rajesh, H.; Hajinur, H.A.; Bilal, A.; Beom, H.S.; Anugya, G.; Vinit, R.; and Lee, S. Repurposing FDA-approved drugs as NLRP3 inhibitors against inflammatory diseases: machine learning and molecular simulation approaches. *J. Biomol. Struct. Dyn.* **2025**, *43*, 4327-4339, https://doi.org/10.1080/07391102.2024.2308072.
22. Alturki, N.A.; Mashraqi, M.M.; Alzamami, A.; Alghamdi, Y.S.; Alharthi, A.A.; Asiri, S.A.; Ahmad, S.; Alshamrani, S. In-Silico Screening and Molecular Dynamics Simulation of Drug Bank Experimental Compounds against SARS-CoV-2. *Molecules* **2022**, *27*, 4391, https://doi.org/10.3390/molecules27144391.
23. Raj, V.; Lee, J.-H.; Shim, J.-J.; Lee, J. Antiviral activities of 4H-chromen-4-one scaffold-containing flavonoids against SARS–CoV–2 using computational and *in vitro* approaches. *J. Mol. Liq.* **2022**, *353*, 118775, https://doi.org/10.1016/j.molliq.2022.118775.
24. Pirolli, D.; Righino, B.; Camponeschi, C.; Ria, F.; Di Sante, G.; De Rosa, M.C. Virtual screening and molecular dynamics simulations provide insight into repurposing drugs against SARS-CoV-2 variants Spike protein/ACE2 interface. *Sci. Rep.* **2023**, *13*, 1494, https://doi.org/10.1038/s41598-023-28716-8.
25. Tang, Y.; Li, X.; Yuan, Y.; Zhang, H.; Zou, Y.; Xu, Z.; Xu, Q.; Song, J.; Deng, C.; Wang, Q. Network pharmacology-based predictions of active components and pharmacological mechanisms of *Artemisia*

annua L. for the treatment of the novel Corona virus disease 2019 (COVID-19). *BMC Complement. Med. Ther.* **2022**, *22*, 56, https://doi.org/10.1186/s12906-022-03523-2.
26. Yasir, M.; Park, J.; Han, E.-T.; Han, J.-H.; Park, W.S.; Chun, W. Investigating the Inhibitory Potential of Flavonoids against Aldose Reductase: Insights from Molecular Docking, Dynamics Simulations, and gmx_MMPBSA Analysis. *Curr. Issues Mol. Biol.* **2024**, *46*, 11503-11518, https://doi.org/10.3390/cimb46100683.
27. Kollman, P.A.; Massova, I.; Reyes, C.; Kuhn, B.; Huo, S.; Chong, L.; Lee, M.; Lee, T.; Duan, Y.; Wang, W.; Donini, O.; Cieplak, P.; Srinivasan, J.; Case, D.A.; Cheatham, T.E. Calculating Structures and Free Energies of Complex Molecules: Combining Molecular Mechanics and Continuum Models. *Acc. Chem. Res.* **2000**, *33*, 889-897, https://doi.org/10.1021/ar000033j.
28. Guan, T.; Bian, C.; Ma, Z. *In vitro* and *in silico* perspectives on the activation of antioxidant responsive element by citrus-derived flavonoids. *Front. Nutr.* **2023**, *10*, 1257172, https://doi.org/10.3389/fnut.2023.1257172.
29. Dey, D.; Hossain, R.; Biswas, P.; Paul, P.; Islam, M.A.; Ema, T.I.; Gain, B.K.; Hasan, M.M.; Bibi, S.; Islam, M.T.; Rahman, M.A.; Kim, B. Amentoflavone derivatives significantly act towards the main protease ($3CL^{PRO}$/M^{PRO}) of SARS-CoV-2: in silico admet profiling, molecular docking, molecular dynamics simulation, network pharmacology. *Mol. Divers.* **2023**, *27*, 857-871, https://doi.org/10.1007/s11030-022-10459-9.
30. Klimoszek, D.; Jeleń, M.; Dołowy, M.; Morak-Młodawska, B. Study of the Lipophilicity and ADMET Parameters of New Anticancer Diquinothiazines with Pharmacophore Substituents. *Pharmaceuticals* **2024**, *17*, 725, https://doi.org/10.3390/ph17060725.
31. John, A.; Umashankar, V.; Krishnakumar, S.; Deepa, P.R. Comparative Modeling and Molecular Dynamics Simulation of Substrate Binding in Human Fatty Acid Synthase: Enoyl Reductase and β-Ketoacyl Reductase Catalytic Domains. *Genomics Inform.* **2015**, *13*, 15–24, https://doi.org/10.5808/GI.2015.13.1.15.
32. Zhao, Z.; Du, J.; Du, Y.; Gao, Y.; Yu, M.; Zhang, Y.; Fang, H.; Hou, X. Deciphering the Allosteric Activation Mechanism of SIRT6 Using Molecular Dynamics Simulations. *J. Chem. Inf. Model.* **2023**, *63*, 5896–5902, https://doi.org/10.1021/acs.jcim.3c00227.
33. Zhang, H.; Zhang, J.; Zhang, H.-X. Effect of quercetin on the protein-substrate interactions in SIRT6: Insight from MD simulations. *J. Mol. Graph. Model.* **2024**, *130*, 108778, https://doi.org/10.1016/j.jmgm.2024.108778.
34. Chauhan, D.; Kumar, S.; Hashim, S.R.; Raj, V. Pharmacophore Generation, Quantitative Structure-Activity Relationship (QSAR), and Molecular Dynamic Simulation of Newly Substituted N-(6- Chloro-3-Cyano-4-Phenyl-4H-Chromen-2-Yl)-2-(4-Chloro-Phenoxy)-Acetamide for Anticancer Activity. *Curr. Comput.-Aided Drug Des.* **2020**, *17*, 504–510, https://doi.org/10.2174/1573409916666200525150410.
35. Rai, A.; Raj, V.; Aboumanei, M.H.; Singh, A.K.; Keshari, A.K.; Verma, S.P.; Saha, S. Pharmacophore, 3D-QSAR Models and Dynamic Simulation of 1,4-Benzothiazines for Colorectal Cancer Treatment. *Comb. Chem. High Throughput Screen* **2017**, *20*, 658–674, https://doi.org/10.2174/1386207320666170509153137.
36. Agarwal, V.; Rehman, M.; Chaudhary, R.; Kaushik, A.S.; Usman, M.; Siddique, M.; Srivastava, S.; Srivastava, S.; Mishra, V. Exploring the Potential of Natural-like Compounds as TNFα Inhibitors: An *In-silico* Approach. *Biointerface Res. Appl. Chem.* **2024**, *14*, 47, https://doi.org/10.33263/BRIAC142.047.
37. Zhu, J.T.T.; Choi, R.C.Y.; Xie, H.Q.; Zheng, K.Y.Z.; Guo, A.J.Y.; Bi, C.W.C.; Lau, D.T.W.; Li, J.; Dong, T.T.X.; Lau, B.W.C.; Chen, J.J.; Tsim, K.W.K. Hibifolin, a flavonol glycoside, prevents β-amyloid-induced neurotoxicity in cultured cortical neurons. *Neurosci. Lett.* **2009**, *461*, 172-176, https://doi.org/10.1016/j.neulet.2009.06.010.
38. Hamsalakshmi, Alex, A.M.; Arehally Marappa, M.; Joghee, S.; Chidambaram, S.B. Therapeutic benefits of flavonoids against neuroinflammation: a systematic review. *Inflammopharmacology* **2022**, *30*, 111–136, https://doi.org/10.1007/s10787-021-00895-8.
39. Wang, Z.; Xue, C.; Yang, T.; Zeng, M.; Wang, Z.; Chen, Q.; Chen, J.; He, Z. Miquelianin, a main functional flavonoid of lotus leaf, induces thermogenic signature via p38-PINK1-PARKIN-mediated mitophagy and mimicking NRF2 signaling during brown adipocyte differentiation. *Food Front.* **2023**, *4*, 1831–1844, https://doi.org/10.1002/fft2.284.
40. Guo, F.; An, J.; Wang, M.; Zhang, W.; Chen, C.; Mao, X.; Liu, S.; Wang, P.; Ren, F. Inhibitory Mechanism of Quercimeritrin as a Novel α-Glucosidase Selective Inhibitor. *Foods* **2023**, *12*, 3415, https://doi.org/10.3390/foods12183415.

41. Bejaoui, A.; M'rabet, Y.; Boulila, A. Caffeoylquinic Acid Derivatives: Chemical Diversity and Effect on the Oxidative Stress-Related Pathologies. *Chem. Afr.* **2024**, *7*, 4105-4126, https://doi.org/10.1007/s42250-024-00985-4.
42. Mooiman, K.D.; Maas-Bakker, R.F.; Moret, E.E.; Beijnen, J.H.; Schellens, J.H.M.; Meijerman, I. Milk Thistle's Active Components Silybin and Isosilybin: Novel Inhibitors of PXR-Mediated CYP3A4 Induction. *Drug Metab. Dispos.* **2013**, *41*, 1494-1504, https://doi.org/10.1124/dmd.113.050971.
43. Dai, J.; Liang, K.; Zhao, S.; Jia, W.; Liu, Y.; Wu, H.; Lv, J.; Cao, C.; Chen, T.; Zhuang, S.; Hou, X.; Zhou, S.; Zhang, X.; Chen, X.-W.; Huang, Y.; Xiao, R.-P.; Wang, Y.-L.; Luo, T.; Xiao, J.; Wang, C. Chemoproteomics reveals baicalin activates hepatic CPT1 to ameliorate diet-induced obesity and hepatic steatosis. *Proc. Natl. Acad. Sci.* **2018**, *115*, E5896-E5905, https://doi.org/10.1073/pnas.1801745115.
44. Ji, J.; Wang, Z.; Sun, W.; Li, Z.; Cai, H.; Zhao, E.; Cui, H. Effects of Cynaroside on Cell Proliferation, Apoptosis, Migration and Invasion though the MET/AKT/mTOR Axis in Gastric Cancer. *Int. J. Mol. Sci.* **2021**, *22*, 12125, https://doi.org/10.3390/ijms222212125.
45. Khajuria, V.; Gupta, S.; Sharma, N.; Tiwari, H.; Bhardwaj, S.; Dutt, P.; Satti, N.; Nargotra, A.; Bhagat, A.; Ahmed, Z. Kaempferol-3-o-β-d-glucuronate exhibit potential anti-inflammatory effect in LPS stimulated RAW 264.7 cells and mice model. *Int. Immunopharmacol.* **2018**, *57*, 62-71, https://doi.org/10.1016/j.intimp.2018.01.041.
46. Xie, Y.; Sun, G.; Tao, Y.; Zhang, W.; Yang, S.; Zhang, L.; Lu, Y.; Du, G. Current advances on the therapeutic potential of scutellarin: an updated review. *Nat. Prod. Bioprospect.* **2024**, *14*, 20, https://doi.org/10.1007/s13659-024-00441-3.
47. Ding, S.; Lu, G.; Wang, B.; Xiang, J.; Hu, C.; Lin, Z.; Ding, Y.; Xiao, W.; Gong, W. Astilbin Activates the Reactive Oxidative Species/PPARγ Pathway to Suppress Effector $CD4^+$ T Cell Activities *via* Direct Binding With Cytochrome P450 1B1. *Front. Pharmacol.* **2022**, *13*, 848957, https://doi.org/10.3389/fphar.2022.848957.
48. Khattulanuar, F.S.; Sekar, M.; Fuloria, S.; Gan, S.H.; Rani, N.N.; Ravi, S.; Chidambaram, K.; Begum, M.Y.; Azad, A.K.; Jeyabalan, S.; Dhiravidamani, A.; Thangavelu, L.; Lum, P.T.; Subramaniyan, V.; Wu, Y.S.; Sathasivam, K.V.; Fuloria, N.K. Tilianin: A Potential Natural Lead Molecule for New Drug Design and Development for the Treatment of Cardiovascular Disorders. *Molecules* **2022**, *27*, 673, https://doi.org/10.3390/molecules27030673.
49. Daina, A.; Michielin, O.; Zoete, V. SwissADME: a free web tool to evaluate pharmacokinetics, drug-likeness and medicinal chemistry friendliness of small molecules. *Sci. Rep.* **2017**, *7*, 42717, https://doi.org/10.1038/srep42717.
50. Agu P.C.; Afiukwa C.A.; Orji O.U.; Ezeh E.M.; Ofoke I.H.; Ogbu C.O.; Ugwuja E.I.; Aja P.M. Molecular docking as a tool for the discovery of molecular targets of nutraceuticals in diseases management. Sci Rep. 2023 Aug 17;13(1):13398. doi: 10.1038/s41598-023-40160-2.
51. Basnet, S.; Ghimire, M.P.; Lamichhane, T.R.; Adhikari, R.; Adhikari, A. Identification of potential human pancreatic *α*-amylase inhibitors from natural products by molecular docking, MM/GBSA calculations, MD simulations, and ADMET analysis. *PLoS ONE* **2023**, *18*, e0275765, https://doi.org/10.1371/journal.pone.0275765.
52. Ivanova, L.; Tammiku-Taul, J.; García-Sosa, A.T.; Sidorova, Y.; Saarma, M.; Karelson, M. Molecular Dynamics Simulations of the Interactions between Glial Cell Line-Derived Neurotrophic Factor Family Receptor GFRα1 and Small-Molecule Ligands. *ACS Omega* **2018**, *3*, 11407–11414, https://doi.org/10.1021/acsomega.8b01524.
53. Gupta, P.; Panwar, U.; Singh, S. Novel scaffolds identification against Mpro of SARS-CoV-2 using shape based screening and molecular simulation methods. *Chem. Phys. Impact* **2024**, *8*, 100496, https://doi.org/10.1016/j.chphi.2024.100496.
54. Deshpande, S.H.; Muhsinah, A.B.; Bagewadi, Z.K.; Ankad, G.M.; Mahnashi, M.H.; Yaraguppi, D.A.; Shaikh, I.A.; Khan, A.A.; Hegde, H.V.; Roy, S. In Silico Study on the Interactions, Molecular Docking, Dynamics and Simulation of Potential Compounds from *Withania somnifera* (L.) Dunal Root against Cancer by Targeting KAT6A. *Molecules* **2023**, *28*, 1117, https://doi.org/10.3390/molecules28031117.
55. Sapundzhi, F.; Popstoilov, M.; Lazarova, M. RMSD Calculations for Comparing Protein Three-Dimensional Structures. In Proceedings of the Numerical Methods and Applications, NMA 2022, Borovets, Bulgaria, August 22–26, 2022; Georgiev, I., Datcheva, M., Georgiev, K., Nikolov, G., Eds.Publisher: Springer, Cham, **2023**; pp. 279-288, https://doi.org/10.1007/978-3-031-32412-3_25.

56. You W.; Zheng W.; Weiss S.; Chua K.F.; Steegborn C. Structural basis for the activation and inhibition of Sirtuin 6 by quercetin and its derivatives. Sci Rep. 2019 Dec 16;9(1):19176. doi: 10.1038/s41598-019-55654-1.
57. Heger V.; Tyni J.; Hunyadi A.; Horáková L.; Lahtela-Kakkonen M.; Rahnasto-Rilla M. Quercetin based derivatives as sirtuin inhibitors. Biomed Pharmacother. 2019 Mar;111:1326-1333. doi: 10.1016/j.biopha.2019.01.035.

Publisher's Note & Disclaimer